Soft Matter

RSC Publishing

PAPER

View Article Online
View Journal | View Issue

Cite this: *Soft Matter*, 2013, **9**, 10811

Effect of chitosan incorporation on the consolidation process of highly hydrated collagen hydrogel scaffolds

Florencia Chicatun,[a] Naser Muja,[a] Vahid Serpooshan,[a] Thomas M. Quinn[b] and Showan N. Nazhat*[a]

Collagenous body tissues exhibit diverse physicochemical and biomechanical properties depending upon their compositions (*e.g.* proteins, polysaccharides, minerals and water). These factors influence cell function and can contribute to tissue dysfunction and disease when they are either deficient or present in excess. Similarly, the constituents of tissue engineering hydrogel scaffolds must be carefully considered for the optimal design of engineered constructs for therapeutic applications. As a natural polysaccharide glycosaminoglycan-analog, chitosan (CTS) holds potential for generating highly hydrated collagen type I hydrogel (Coll) based scaffolds that mimic the native extracellular matrix. Analysis of fluid loss in Coll–CTS hydrogels undergoing either a gravity-driven consolidation process (self-compression; SC) or plastic-compression (PC) offers the potential for the controlled production of tissue-equivalent dense hydrogels with tailored physical and mechanical properties. Herein, the effect of CTS on Coll gels microstructural evolution involved in SC and PC was investigated by detecting the spatiotemporal distribution of fluorescent beads within Coll–CTS hydrogels using confocal microscopy. The hydraulic permeability (k), pre- and post-consolidation, as a function of CTS content, was estimated by the Happel model. The effect of CTS fixed charge on dense Coll–CTS hydrogels was investigated through structural, mechanical and swelling characterizations under isotonic and hypertonic conditions. Image analysis revealed a temporal increase in bead density, with both rate and extent of consolidation, correlating strongly with increasing CTS content. k decreased from 1.4×10^{-12} to 1.8×10^{-13} m^2 and from 2.9×10^{-14} to 6.8×10^{-15} m^2 for highly hydrated and dense hydrogels, respectively, with higher amount of CTS, resulting in a concomitant increase in the scaffold compressive modulus (from 7.65 to 14.89 kPa). In summary, understanding the effect of CTS on Coll hydrogel properties enables the development of tailored scaffolds for use as tissue models for various biomedical applications.

Received 12th August 2013
Accepted 20th September 2013

DOI: 10.1039/c3sm52176a

www.rsc.org/softmatter

1. Introduction

Tissue engineering (TE) aims to design and develop scaffolds that model the complex structure of native tissues and support the growth and differentiation of relevant cells for therapeutic applications.[1] The availability of constructs with well-defined chemical composition, physical structure and biological functions is critical for improved understanding of the intricate mechanisms underlying physiological and pathophysiological processes, while also providing a bridge between animal models of disease and clinical studies.[2] Therefore, the success of three-dimensional (3D) tissue models depends upon the control of multiple biophysical parameters, including microstructure, hydraulic permeability (k), as well as biomechanical and swelling properties.

Type I collagen (Coll) is the major determinant of the structural and functional properties of connective tissues and has been extensively used as 3D biomimetic scaffolds for diverse biomedical applications.[3,4] In particular, Coll-based hydrogels offer biochemical and biomechanical signals that mimic the extracellular matrix (ECM) of tissues, providing an excellent *in vitro* tissue model. In addition to the complex dense fibrillar network of collagen, connective tissues are also comprised of additional biomacromolecules that contribute to the diverse physicochemical properties of tissues, such as non-fibrillar proteins and proteoglycans containing charged glycosaminoglycan (GAG) side chains surrounded by interstitial fluid, as well as mineral, in the case of bone and calcified cartilage.[5,6] Indeed, the repulsive electrostatic forces between the negatively charged GAGs entrapped within the collagen meshwork are directly responsible for the stiffness and swelling of the ECM.[7,8]

Chitosan (CTS) is an abundant cationic polysaccharide composed of a disaccharide repeating unit,[9,10] which has been demonstrated to be biocompatible, biodegradable, with antibacterial, wound healing and bioadhesive characteristics.[11]

[a]*Department of Mining and Materials Engineering, McGill University, Montreal, Quebec, Canada H3A 2B2. E-mail: showan.nazhat@mcgill.ca*

[b]*Department of Chemical Engineering, McGill University, Montreal, Quebec, Canada H3A 2B2*

Since CTS is a natural biopolymer that resembles the structure, composition and biological activity of native GAGs,[12–15] it is hypothesized herein that modulation of its content within highly hydrated Coll hydrogels holds potential for engineering 3D tissue models with tailored biophysicochemical properties.

Reconstituted Coll–CTS hydrogels have been widely investigated as *in vitro* tissue models and as 3D scaffolds for several TE applications.[16–20] However, highly hydrated Coll–CTS hydrogels are predominately comprised of unbound water (>99 wt%) and collapse due to their unstable physical structure in the absence of external support.[16,21] This gravitational force-driven process – identified as self-compression (SC) – allows for the expulsion of the unbound water (>95 wt%) that results from casting. SC can be accelerated through the controlled application of an external load (plastic compression; PC) in order to rapidly generate scaffolds with physiologically relevant collagen fibrillar densities (~8%).[21,22] PC has been recognized as an efficient processing method for the generation of tissue equivalent cell-seeded dense Coll gels with greatly enhanced mechanical strength.[21] A number of studies have described the microstructural evolution of Coll hydrogels undergoing SC or PC, with varied theoretical models estimating their k.[23–25] However, the effect of a charged polysaccharide, such as CTS, on the consolidation process of highly hydrated Coll hydrogels has not been investigated. In this study, Coll–CTS hydrogels, having relative compositions of 1 : 0, 2 : 1 and 1 : 1 (w/w), were uniformly seeded with fluorescent beads and subjected to SC or PC. Serial confocal laser scanning microscopy was used to determine the microstructural evolution of Coll–CTS hydrogels undergoing consolidation by collecting 3D image stacks of the spatiotemporal distribution of the fluorescent beads during the collapse process. The Happel model for flow through a random array of long cylindrical fibres was used to theoretically predict k of pre- and post-compressed hydrogel.[26] In addition, compressive mechanical testing evaluated the relationship between k and compressive modulus of dense gels. Finally, the effect of CTS fixed charge on the structural, mechanical and swelling properties of dense Coll–CTS hydrogels and its contribution to k was investigated under isotonic and hypertonic conditions for charge screening. The incorporation of CTS within dense Coll hydrogels was found to modify the biophysicochemical properties of the hydrogel, providing a reliable 3D *in vitro* tissue model that may be adapted to optimize TE scaffold design and improve therapeutic outcomes.

2. Materials and methods

2.1. Preparation of Coll and Coll–CTS hydrogel scaffolds

Ultrapure CTS powder (79.8% DDA, Ultrasan™, BioSyntech Ltd., Montreal, QC, Canada (now Piramal Healthcare, Laval, QC, Canada)) was dissolved in 0.1 M acetic acid at 4 °C and stirred overnight. Coll–CTS mixtures were prepared by blending sterile, rat-tail tendon-derived collagen type I (2.10 mg ml^{-1} of protein in 0.6% acetic acid, First Link Ltd., West Midlands, UK) and CTS at Coll–CTS weight ratios of 2 : 1 and 1 : 1, as previously described.[16,27] Coll and Coll–CTS self-assembly was achieved by mixing the solution with 10× Minimum Essential Medium (MEM, Sigma Aldrich, Ottawa, ON, CA) at a ratio of 4 : 1 and by adjusting the solution pH to 7.4 with 5 M NaOH. Neutralized Coll or Coll–CTS solutions were pipetted into four-well plates (0.9 ml per well of 4.5 mm height × 16 mm diameter) to generate circular discs of highly hydrated gels. Gelation was achieved by allowing the solutions to set at 37 °C in a 5% CO_2 incubator for 30 min.

2.2. Unidirectional self- and plastic-compression of Coll and Coll–CTS hydrogels

Highly hydrated gels were transferred to an impermeable polystyrene tube (16 mm diameter) for radial confinement on a substrate consisting of a stack of metal and nylon meshes and water-saturated paper blot. The tube allowed for unidirectional fluid flow out of the gel in the z direction, parallel to the driving force for flow. The wet substrate was maintained at the level of a water bath to allow for gravity driven fluid flow and avoid capillary effect. Hydrogels were allowed to undergo unidirectional SC up to 40 min or PC up to 5 min, until equilibrium was reached, using a compressive stress of 0.5 kPa at room temperature in a closed chamber maintained at 100% humidity.

Gel weight, initially (w_0) and at various time points (w_t) during SC or PC, was measured with a digital analytical balance ($n = 4$; Mettler-Toledo AE 163, readability of 0.01 mg; Switzerland). Weight loss (%) was calculated using:

$$\text{Weight loss } (\%) = \frac{w_0 - w_t}{w_0} \times 100 \quad (1)$$

Pre- and post-compression solid weight percent were also verified through freeze-drying (BenchTop K freeze dryer, VirTis, SP Industries, Gardiner, NY, USA), as follows:

$$\text{Solid weight percent} = \frac{\text{Total solid content (g)}}{\text{Total solid content (g)} + \text{water (g)}} \times 100 \quad (2)$$

2.3. Microstructural evolution of Coll and Coll–CTS hydrogels undergoing consolidation

The microstructural evolution of Coll and Coll–CTS hydrogels undergoing either SC or PC was analyzed by monitoring the spatiotemporal distribution of green-fluorescent beads (2 μm in diameter, FluoSpheres® carboxylate-modified microspheres, 2% solids, Molecular Probes®, Oregon, USA) incorporated into the hydrogels by confocal laser scanning microscopy (CLSM, Carl Zeiss, LSM5 Exciter, Toronto, ON, CA). These carboxylate-modified fluorescent beads present carboxylic acids that can covalently link to amine-containing molecules, such as Coll and CTS, therefore ensuring that fluorescent bead position is a reliable marker of solid density. Encapsulation of the beads was achieved immediately after Coll or Coll–CTS solution neutralization. Briefly, after physiological pH (7.4) was attained, the fluorescent beads were sonicated for 3 min and added using a volume ratio of 1 : 450. The gel suspension was then further sonicated for 2 min at 4 °C to avoid gel polymerization and allow a homogeneous bead distribution. After gelation for 30 min at 37 °C, highly hydrated gels were allowed to undergo SC or PC, as described above.

At 0, 5, 20 and 40 min of SC and 0, 1, 3 and 5 min of PC, gels were immediately fixed by immersion in 0.1 M sodium cacodylate buffer containing 4% paraformaldehyde and 2% glutaraldehyde and left overnight. Following fixation, gels were washed with phosphate buffered saline (PBS; 3 × 10 min) and transferred to a glass dish (35 mm in diameter, MatTek, Ashland, MA, USA) for CLSM analysis ($n = 3$). Three-dimensional image stacks of Coll and Coll–CTS hydrogels were acquired at 1 Airy unit using a 10× objective (EC Plan Neofluoar; 0.3 NA) and argon excitation (488 nm). Image slice thickness was set to 10 μm with an image area of 1264 × 1264 μm. Orthogonal images of hydrogel scaffolds were generated using Zeiss LSM image browser (Carl Zeiss Inc., *v*.4.4.0.121, Germany). The number of beads in each slice was determined by transforming each slice into a binary image and performing automatic particle counting using the Analyze Particle tool in ImageJ software (1.42q, Rasband W, National Institutes of Health, Bethesda, MD, USA).

Three different regions were selected to describe the microstructural evolution of Coll gels during confined SC and PC: top 20 μm, bottom 20 μm and bottom 80 μm of the gel; with the bottom part of the gel being the fluid expulsion boundary (FEB) where the fluid flows through. The rationale for the selection of these regions was based on previous studies on Coll gels undergoing consolidation showing the formation of a dense lamella that progressively thickens from the basal surface towards the upper surface of the gel (~80 μm at the equilibrium state), in analogy to the compaction of materials at ultrafiltration surface.[23,24]

Bead density (ρ_{bead}) was calculated by dividing the total number of beads in the top 20 μm, bottom 20 μm and bottom 80 μm of the hydrogel by the analyzed volume ((20 or 80) × 1264 × 1264 μm^3). The fold increase in density was calculated as follows:

$$\text{Fold increase in density} = \frac{\rho_{bead}}{\rho_{HHG}} \quad (3)$$

where ρ_{HHG} is the initial density of the highly hydrated gels ($t = 0$).

2.4. Hydraulic permeability of Coll and Coll–CTS hydrogels

The hydraulic permeability (k) of highly hydrated and dense gels generated by unidirectional SC or PC, were calculated using the Happel model for flow through a random array of long cylindrical fibres.[26,28] This model may be summarized as follows:

$$k = \frac{2}{3}k_{\perp} + \frac{1}{3}k_{\parallel} \quad (4)$$

where $k_{\perp}$ and $k_{\parallel}$ are the contributions of the perpendicular and parallel fibres to permeability[5,26] as a function of the rod hydrodynamic radius (a) and the gel solid volume fraction (σ):

$$k_{\perp} = \frac{a^2}{8}\left[\frac{1}{\sigma}\ln\left(\frac{1}{\sigma}\right) - \frac{1}{\sigma}\frac{1-\sigma^2}{1+\sigma^2}\right] \quad (5)$$

and

$$k_{\parallel} = \frac{a^2}{8}\left[4 - \sigma + \frac{1}{\sigma}\left\{2\ln\left(\frac{1}{\sigma}\right) - 3\right\}\right] \quad (6)$$

σ of Coll and Coll–CTS was determined as follows:

$$\sigma = \frac{\text{Solid mass(g)}}{\text{Vol}_{liquid}(\text{cm}^3) \times \rho\left(\frac{\text{g}}{\text{cm}^3}\right)} \quad (7)$$

Coll and CTS bulk densities (ρ) of 1.41 and 0.32 g cm^{-3},[29,30] respectively, along with the weight of solid and liquid obtained from the weight loss data and freeze-dried scaffolds pre- and post-compression, were used to calculate σ. For Coll–CTS hydrogels it was assumed that CTS was the most critical determinant of k and responsible for the high hydraulic resistance in the hydrogel, in analogy to the GAG chains found in cartilage which lace the interstitial space;[10] thus the totality of the fluid within the Coll–CTS hydrogel was solely associated with CTS for the calculation of σ. k of the hydrogels was calculated using a collagen fibrillar radius of 50 nm,[28] measured through electron microscopy investigations and using a hydrodynamic CTS radius of 39 nm.[31] Rod radius was assumed to be constant for all gel specimens.

The electrokinetic effect of the positively charged CTS on k of dense Coll–CTS gels was evaluated by screening its fixed charge in a saline solution of high salt concentration (hypertonic; 1.5 M NaCl), and compared to an isotonic solution (0.15 M NaCl) and non-conditioned samples (control).[32,33] As-prepared highly hydrated Coll–CTS gels were immediately placed in the saline solution to avoid a gravity-driven collapse, which is eliminated by the buoyancy force of the fluid. Highly hydrated gels were conditioned for 1 day to allow for Donnan equilibrium and then subjected to unidirectional PC. Weight loss was gravimetrically measured to calculate σ using eqn (4). k of uncharged hydrogels was calculated using eqn (4)–(6).

2.5. Mechanical analysis of dense Coll and Coll–CTS hydrogels

Unconfined compressive mechanical tests were conducted on dense cylindrical rolls using a displacement actuator (LTA-HL, Newport, Irvine, CA, USA) mounted in a rigid frame and interfaced to a PC (LabVIEW) equipped with a 50 g-load cell (Model 31, Honeywell, Golden Valley, MN, USA).[34] The apparatus was mounted on an antivibration table (Newport), covered by a plexiglass box and surrounded with thermal insulation (T = 23 °C). All measurements were conducted in displacement control with a cross-head speed of 0.005 mm s^{-1}. Spiral constructs were used to facilitate better handling. For this purpose, 4.5 ml of Coll or Coll–CTS solution was pipetted into a rectangular mold (18 × 40 × 6.2 mm^3), let set at 37 °C and subjected to unidirectional PC as described above. Cylindrically shaped rolls (2.97 ± 0.09, 4.34 ± 0.35 and 5.27 ± 0.17 mm diameter; and 3.65 ± 0.45, 4.12 ± 0.37 and 3.91 ± 0.30 mm height for Coll, Coll–CTS 2 : 1 and Coll–CTS 1 : 1, respectively) were obtained by cutting the rectangular sheet in half through the short axis (9 mm width × 40 mm length × 150 to 250 μm thick), plying through the middle along the short axis and rolling along their long axis. The specimen diameter was measured using a stereomicroscope (Zeiss Stemi 2000-C) equipped with a digital camera (Canon Powershot A640) attached to a tube adapter (Zeiss MC80DX 1.0). Cylindrically

shaped rolls were conditioned by immersing the scaffolds in an isotonic or hypertonic solution for 1 day and compressed using a stainless steel plunger up to 80% strain without any evidence of specimen unfolding ($n = 3$). The stress was calculated by normalizing the recorded force against the initial resistance area of the specimen, and the strain was calculated by normalizing the displacement against the initial height of the specimen. The compressive modulus values were computed from the slope of the initial linear region of the stress-strain outputs.[16,35]

2.6. Swelling properties of dense Coll and Coll–CTS in saline solutions

Dense Coll and Coll–CTS gels were produced by unconfined PC, as described above, and immediately transferred to either an isotonic or hypertonic solution. Gels were allowed to move freely within the bath. At specific time points, up to 60 min, gels ($n = 4$) were removed from the bath with a L-shaped metal mesh and the excess fluid was absorbed using blotting paper, weighed and returned to the bath. Gel weight was recorded over time and the swelling ratio was determined as follows:[36]

$$\text{Swelling ratio } (\%) = \frac{(w_t - w_0)}{w_0} \times 100 \qquad (8)$$

where w_0 and w_t are the gel initial weight (post-compression) and weight at time t, respectively.

2.7. Statistical analysis

All data are presented as mean values ± standard deviation of the mean (±SD). Statistical significance between scaffold groups and between time points was determined using a one-way ANOVA with a Tukey–Kramer's *post-hoc* multiple comparison of means. The level of statistical significance was set at $p = 0.05$.

3. Results

3.1. Effect of CTS on the consolidation process of Coll hydrogels undergoing unidirectional SC and PC

To investigate the microstructural evolution of highly hydrated hydrogels undergoing consolidation following the initiation of SC (Fig. 1) or PC (Fig. 2), CLSM was carried out to monitor the distribution of fluorescent beads throughout the thickness of Coll and Coll–CTS gels at defined time points. Representative orthogonal images of the z–y and x–z planes of gel specimens are shown for each hydrogel formulation in Fig. 1A_i–C_i. CLSM orthogonal images confirmed the homogeneous fluorescent bead distribution throughout the initial ($t = 0$) 2.5 mm thickness of highly hydrated gels. The extent of reduction in gel thickness at the equilibrium state (40 min SC) significantly decreased ($p < 0.05$) with CTS content, reaching 120 ± 8.2, 167 ± 4.7 and 200 ± 21.6 μm for Coll (Fig. 1A_{ii}), Coll–CTS 2 : 1 (Fig. 1B_{ii}) and Coll–CTS 1 : 1 (Fig. 1C_{ii}), respectively. A similar trend was observed after 5 min of PC, where gel thicknesses of 96.7 ± 9.4, 103 ± 12.5 and 150 ± 16.3 μm were generated for Coll (Fig. 2A_{ii}), Coll–CTS 2 : 1 (Fig. 2B_{ii}) and Coll–CTS 1 : 1 (Fig. 2C_{ii}), respectively. There was a significant difference between the final thickness of Coll and Coll–CTS 2 : 1 with Coll–CTS 1 : 1 gels ($p < 0.05$). Analysis of z-stack images during SC and PC of highly hydrated gels revealed an incremental bead accumulation in both the top and bottom regions over time attributable to matrix densification (Fig. 3). Regions of 20 μm thickness at the top and bottom of the hydrogels undergoing SC (Fig. 3A–C) and PC (Fig. 3D–F) were analyzed, based upon previous studies that describe the formation of a dense lamella at the FEB of Coll hydrogels, in order to measure changes in ρ_{bead} over time.[23] In addition, a bottom 80 μm thickness region (comprising the bottom 20 μm) was also investigated.

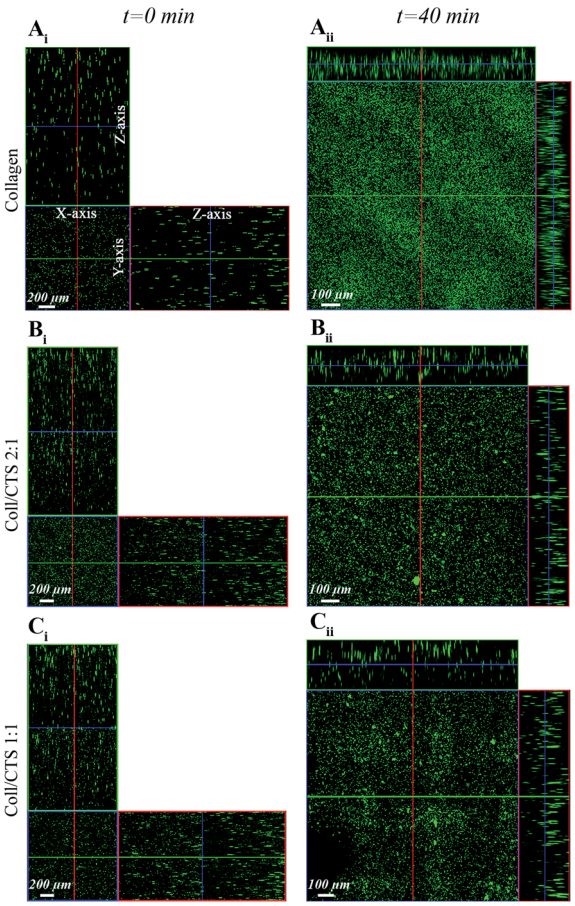

Fig. 1 CLSM detection of fluorescent bead distribution within Coll and Coll–CTS hydrogels following SC. *Ortho*-representation of the confocal z-stacks throughout the entire thickness of Coll (A_i), Coll–CTS 2 : 1 (B_i) and Coll–CTS 1 : 1 (C_i) hydrogels reveals an initial uniform distribution of fluorescent beads within the gel scaffolds immediately prior to SC ($t = 0$; scale bar = 200 μm). After 40 min of SC, the thicknesses of the gel scaffolds decreased to 120 ± 8.2, 167 ± 4.7 and 200 ± 21.6 μm for Coll (A_{ii}), Coll–CTS 2 : 1 (B_{ii}) and Coll–CTS 1 : 1 (C_{ii}), respectively. Scale bar = 100 μm.

After 5 min SC, ρ_{bead} within the bottom 20 μm of Coll constituted 66% of the final density (Fig. 3A). There was no significant difference in ρ_{bead} between 20 and 40 min within the bottom 20 μm ($p > 0.05$). The z-stack analysis revealed that the ρ_{bead} at the bottom 80 μm followed the same trend, however the ρ_{bead} was 12.7% lower than that of the bottom 20 μm. While ρ_{bead} within the top 20 μm exhibited a slower rate of increase when compared to that within the bottom 20 μm, after 40 min of SC it reached a similar value to ρ_{bead} within the bottom

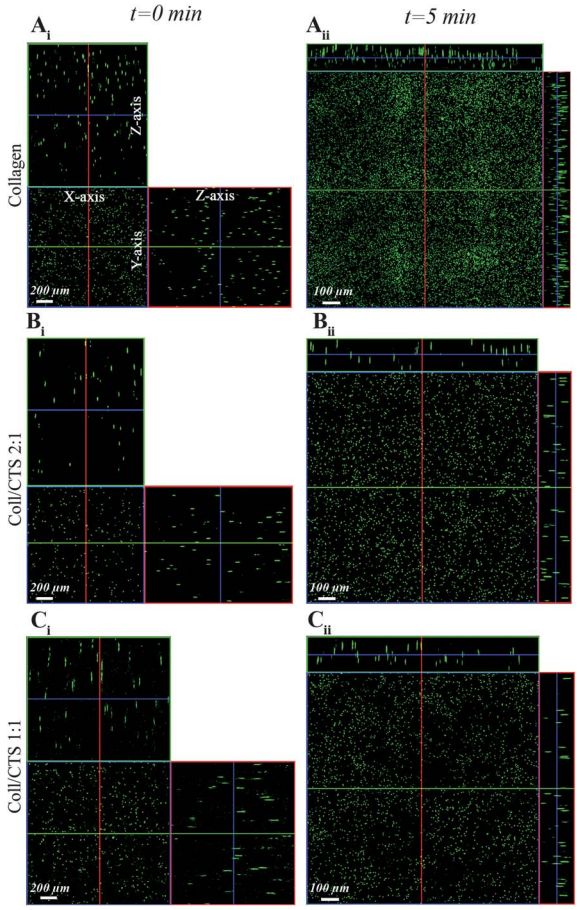

Fig. 2 CLSM detection of fluorescent bead distribution within Coll and Coll–CTS hydrogels undergoing PC. *Ortho*-representation of the confocal z-stacks throughout the entire thickness of Coll (A_i), Coll–CTS 2 : 1 (B_i) and Coll–CTS 1 : 1 (C_i) hydrogels reveals an initial uniform distribution of fluorescent beads within the gel scaffolds ($t = 0$; scale bar = 200 μm). After 5 min of application of an external stress of 0.5 kPa for 5 min, the gel thickness decreased to 96.7 ± 9.4, 103 ± 12.5 and 150 ± 16.3 μm thickness in Coll (A_{ii}), Coll–CTS 2 : 1 (B_{ii}) and Coll–CTS 1 : 1 (C_{ii}), respectively. Scale bar = 100 μm.

80 μm. For Coll–CTS hydrogels, ρ_{bead} within the bottom 20 and 80 μm regions equilibrated within 5 min of SC (Fig. 3B and C). Relative to Coll, there was a decrease in ρ_{bead} within both top and bottom regions with an increase in CTS content. After 40 min SC, ρ_{bead} within the top 20 μm regions were 73, 28 and 24% the value of ρ_{bead} within the bottom 20 μm regions of Coll, Coll–CTS 2 : 1 and 1 : 1 hydrogels, respectively. Also after 40 min SC, the bottom 80 μm regions underwent a 40.3 ± 0.6, 15.7 ± 1.7 and 11.9 ± 0.9 fold increase in ρ_{bead} in the case of Coll, Coll–CTS 2 : 1 and 1 : 1, respectively, compared to the initial ρ_{bead} of the highly hydrated gels ($t = 0$).

Analysis of z-stack images during PC (Fig. 3D–F) revealed an incremental bead accumulation within both top and bottom regions as early as 1 min, with the bottom 20 μm region of all hydrogels reaching a stable ρ_{bead} value. After 3 min, ρ_{bead} within the bottom 80 μm of Coll gels equilibrated. While Coll–CTS 2 : 1 exhibited a similar trend, Coll–CTS 1 : 1 showed no statistical difference at the bottom 80 μm between all time points ($p > 0.05$). Similar to SC, ρ_{bead} in both top and bottom regions of the gels decreased with CTS content, where the final ρ_{bead} within the bottom 80 μm of Coll, Coll–CTS 2 : 1 and 1 : 1 underwent a 35.8 ± 3.7, 21.3 ± 2.2 and 18.0 ± 1.8 fold increase, respectively. However, and in contrast to SC, there was no statistical difference in ρ_{bead} in hydrogels undergoing PC between top and bottom regions at the equilibrium state ($p > 0.05$).

3.2. Weight loss and *k* of Coll and Coll–CTS hydrogels

Weight loss of highly hydrated gels was measured as a function of unidirectional SC (Fig. 4A) or PC (Fig. 4B). Under both conditions there was an initial rapid rate of weight loss, which was followed by a gradual reduction in weight loss towards an equilibrium state. Increasing amounts of CTS resulted in a decrease in the initial weight loss rate. After 40 min SC there was a 41.1 ± 4.1, 13.4 ± 0.6 and 9.5 ± 0.5 fold increase in solid weight percent for Coll, Coll–CTS 2 : 1 and 1 : 1, respectively, compared to the initial state ($t = 0$). The final solid weight percent of the hydrogels after 5 min of PC followed a similar trend, with the percentages decreasing with higher CTS content (42.0 ± 1.4, 23.0 ± 2.3 and 14.3 ± 0.2 fold increase for Coll, Coll–CTS 2 : 1 and 1 : 1, respectively).

The Happel model was used to calculate k for all hydrogels pre- and post-compression by using the weight loss and σ values (Table 1), along with the reported hydrodynamic radius of collagen and CTS fibres (Fig. 4C and D). k decreased with increasing CTS content resulting in 1.4×10^{-12} ($\pm 1.1 \times 10^{-13}$), 3.9×10^{-13} ($\pm 1.1 \times 10^{-14}$) and 1.8×10^{-13} ($\pm 3.4 \times 10^{-15}$) m^2 for Coll, Coll–CTS 2 : 1 and 1 : 1, respectively. A similar trend was observed for the dense hydrogels, with k decreasing from 2.7×10^{-14} ($\pm 2.5 \times 10^{-15}$), 1.6×10^{-14} ($\pm 5.2 \times 10^{-16}$) and 9.5×10^{-15} ($\pm 2.1 \times 10^{-16}$) m^2 for SC and 2.9×10^{-14} ($\pm 2.7 \times 10^{-15}$), 1.5×10^{-14} ($\pm 5.2 \times 10^{-16}$) and 6.8×10^{-15} ($\pm 1.6 \times 10^{-16}$) m^2 for PC for Coll, Coll–CTS 2 : 1 and Coll–CTS 1 : 1, respectively.

3.3. Electrokinetic effect of CTS on *k* of dense Coll hydrogels

PC-induced weight loss of Coll and Coll–CTS hydrogels was evaluated by immersing as prepared highly hydrated gels in a hypertonic solution for charge screening (Fig. 5A–C) and compared to those in an isotonic solution and non-conditioned hydrogels (control). After 5 min PC in isotonic solution, there was a 95.0 ± 0.2, 91.7 ± 1.4 and 91.1 ± 0.5% weight loss for Coll, Coll–CTS 2 : 1 and 1 : 1, respectively. The weight loss of Coll–CTS hydrogels pre-conditioned in hypertonic solution increased with CTS content (95.16 ± 0.90, 93.96 ± 0.35% and 92.85 ± 0.44% for Coll, Coll–CTS 2 : 1 and 1 : 1, respectively), and was higher when compared to those in isotonic solution. No statistical difference was observed in the percentage weight loss of Coll between isotonic and hypertonic solutions ($p > 0.05$). Moreover, there was no statistical difference in the percentage weight loss of all formulations between control and isotonic condition.

Weight loss data was used to calculate σ of dense hydrogels under both conditions and applied into eqn (4–6) to predict the effect of CTS fixed charge on k (Fig. 5D). There was no statistical difference ($p > 0.05$) between the k of Coll when pre-conditioned in either isotonic or hypertonic solutions. However, there was a

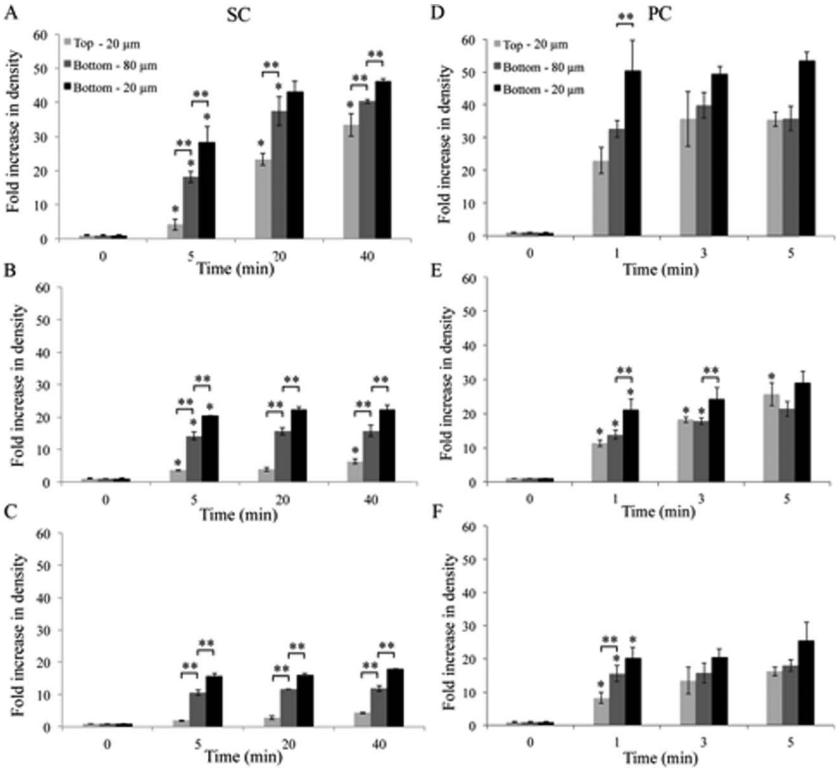

Fig. 3 Effect of CTS on Coll hydrogel consolidation by SC and PC. The spatiotemporal distribution of fluorescent beads was studied by CLSM as an indicator of the structural evolution of highly hydrated hydrogels when undergoing compression. ρ_{bead} within the top 20 μm and bottom 20 and 80 μm of Coll (A and D), Coll–CTS 2 : 1 (B and E) and Coll–CTS 1 : 1 (C and F) undergoing SC (A–C) and PC (D–F). Analysis of the collapse process was evaluated after 5, 20 and 40 min of the initiation of the gravity-driven process and after application of an external load for 1, 3 and 5 min. After 40 min of SC, there was a 40.3 ± 0.6, 15.7 ± 1.7 and 11.9 ± 0.9 fold increase in ρ_{bead} within the bottom 80 μm of dense Coll, Coll–CTS 2 : 1 and Coll–CTS 1 : 1 gels, respectively. The ρ_{bead} within the bottom 80 μm of all samples were significantly different ($p < 0.05$). After 5 min of PC, there was a 35.8 ± 3.7, 21.3 ± 2.2 and 18.0 ± 1.8 fold increase fold increase in ρ_{bead} within the bottom 80 μm of dense Coll, Coll–CTS 2 : 1 and Coll–CTS 1 : 1 gels, respectively. There was no significant difference between ρ_{bead} within the bottom 80 μm of dense Coll–CTS 2 : 1 and Coll–CTS 1 : 1 ($p > 0.05$). A significant difference in ρ_{bead} within the bottom 80 μm was observed between Coll and Coll–CTS hydrogels ($p < 0.05$). Both ρ_{bead} after SC or PC were in line with the fold increase in solid weight percent post-compression (42.0 ± 1.4, 23.0 ± 2.3 and 14.3 ± 0.2 fold). Hydrogels undergoing PC showed no statistical difference between top and bottom densities at the equilibrium state ($p > 0.05$). Data represented as mean ± SD, $n = 3$. * indicates a significant difference ($p < 0.05$) compared to previous time point. ** indicates a significant difference ($p < 0.05$) compared to a different region at the considered time point.

significant decrease ($p < 0.05$) in k of Coll–CTS hydrogels pre-conditioned in hypertonic solution.

The compressive modulus, calculated from the initial region of the stress-strain curves of dense hydrogels, tested after a 1 day pre-conditioning period in isotonic (7.65 ± 1.67, 9.94 ± 0.68 and 14.89 ± 1.53 kPa for Coll, Coll–CTS 2 : 1 and 1 : 1, respectively) and hypertonic solutions (7.50 ± 2.55, 8.68 ± 0.53 and 16.81 ± 1.71 kPa for Coll, Coll–CTS 2 : 1 and 1 : 1, respectively) significantly increased with CTS content. There was no statistical difference in the compressive modulus of Coll, Coll–CTS 2 : 1 and Coll–CTS 1 : 1 when pre-conditioned in isotonic or hypertonic solutions ($p > 0.05$). The increase in compressive modulus with CTS content corresponded with a decrease in the k of the hydrogels (Fig. 6).

3.4. Swelling of dense Coll and Coll–CTS hydrogels in isotonic and hypertonic solutions

The weight change due to water absorption of dense Coll and Coll–CTS gels was measured in either isotonic or hypertonic solutions to evaluate the electrostatic contribution of CTS to Coll hydrogels swelling properties (Fig. 7). The swelling of all hydrogels reached equilibrium within 5 min. Pairwise comparisons (ANOVA, $p < 0.05$) of each group of hydrogels in both solutions showed that the swelling ratio of Coll–CTS 2 : 1 and Coll–CTS 1 : 1 decreased with an increase in salt concentration, while that of Coll remained unchanged. In particular, in isotonic solution, equilibrium swelling ratio significantly increased ($p < 0.05$) with increasing CTS content, demonstrating a 48 ± 4, 88 ± 9 and 107 ± 10% increase for Coll, Coll–CTS 2 : 1 and 1 : 1, respectively. In contrast, in hypertonic solution, there was no statistical difference ($p > 0.05$) between the equilibrium swelling ratio of Coll (49 ± 3%) when compared to that of Coll–CTS 2 : 1 (49 ± 5%), while that of Coll–CTS 1 : 1 was significantly lower ($p < 0.05$).

4. Discussion

The distinct physicochemical properties of the 3D *in vivo* extracellular microenvironment demand the development of biomimetic scaffolds with optimal characteristics. Coll–CTS

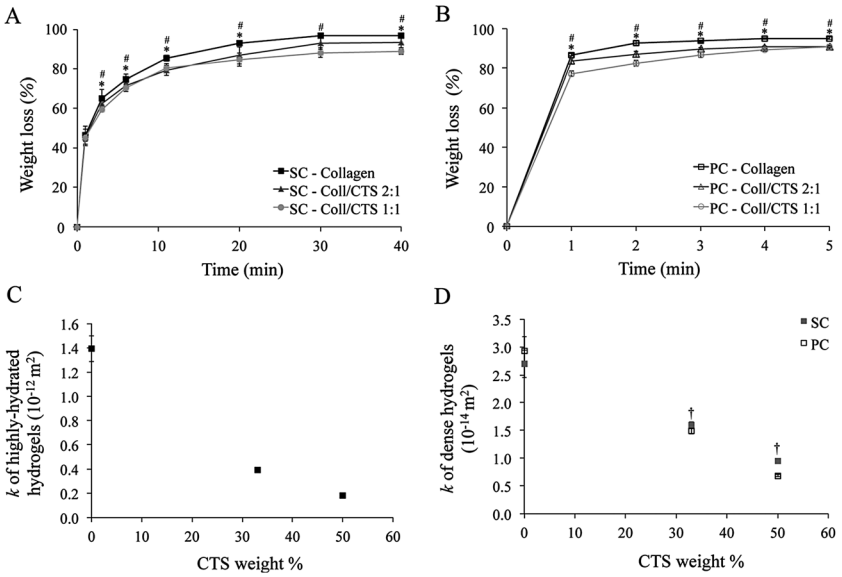

Fig. 4 Effect of CTS on weight loss and hydraulic permeability (k) of Coll and Coll–CTS hydrogels under unidirectional SC and PC. Analysis of the effect of CTS on weight loss due to fluid expulsion and hydraulic permeability calculated using the Happel model measured up to 40 min SC and 5 min PC. Experimental data for weight loss during SC (A) and PC (B) were used to determine k for highly hydrated (C) and dense hydrogels (D) which underwent SC or PC. There was a decrease in k with CTS content. Data represented as mean ± SD, $n = 3$. * indicates a significant difference ($p < 0.05$) between Coll and Coll–CTS 2 : 1. # Indicates a significant difference ($p < 0.05$) between Coll and Coll–CTS 1 : 1. † Indicates a significant difference ($p < 0.05$) between SC and PC.

hydrogels provide an excellent ECM-mimetic milieu for cell growth and differentiation.[16–20] Modulation of CTS within the Coll fibrillar structure exhibits great potential for the development of scaffolds with tailored physicochemical properties directed towards TE and drug delivery applications. However, highly hydrated Coll–CTS hydrogels present insufficient mechanical strength and poor structural integrity on account of the unbound water that results from hydrogel casting.[21] Under unconfined conditions, highly hydrated Coll hydrogels undergo a gravity-driven SC process governed by interstitial fluid flow within the porous fibrillar matrix, which is accelerated by an external compressive stress (PC) to produce dense hydrogels with fibrillar densities approaching those of native ECM.[16,21,22] However, the effect of CTS incorporation on the microstructural evolution of Coll–CTS hydrogels undergoing consolidation either through SC or PC has not been investigated. Having the means to understand this effect would enable greater control of hydrogel microstructure, which ultimately allows for a greater range of properties (*e.g.* hydraulic permeability, mechanics and swelling) that can be tailored to meet specific requirements for each target application.

Coll–CTS of relative compositions of 1 : 0, 2 : 1 and 1 : 1 (w/w) were prepared to approach the weight ratios of Coll/GAGs in the native ECM of tissues (*e.g.* bone osteoid, cartilage, tendon and ligaments).[6,16,37] The consolidation process through either SC or PC of highly hydrated Coll–CTS hydrogels was characterized by monitoring the distribution of fluorescent beads over time by CLSM. Previously, studies have determined that Coll hydrogels consist of two distinct layers following SC and PC: a highly hydrated or bulk layer, and an underlying dense lamella.[23,24] In analogy to the compaction of materials at ultrafiltration surfaces, the basal surface of the Coll hydrogel serves as the principal FEB, retaining the collagen fibrils.[21] In particular, Serpooshan *et al.*[24] reported that after 1 minute undergoing SC, the basal surface of the Coll hydrogel develops into a 20 μm dense lamella, which increases in thickness until reaching 80 μm at the equilibrium state. Therefore, based upon these data, the top 20 μm, the bottom 20 μm and 80 μm were selected for further analysis. In the current work, 3D maximum intensity CLSM projections attested an initial homogeneous bead distribution throughout the entire thickness of highly hydrated hydrogels. Image analysis revealed a temporal

Table 1 Weight loss and solid volume fraction (σ) of Coll and Coll–CTS gel scaffolds attributable to SC and PC. σ was calculated based on gravimetric analysis of freeze-dried scaffolds pre- and post-compression and weight loss data. Values are presented as the mean ± standard deviation

	Highly hydrated	Self-compression (SC)		Plastic compression (PC)	
Sample	σ_{HHG}	Weight loss (%)	σ_{SC}	Weight loss (%)	σ_{pc}
Collagen	0.0016 ± 0.0001	95.4 ± 0.5	0.0325 ± 0.0006	95.1 ± 0.6	0.0320 ± 0.0022
Coll–CTS 2 : 1	0.0030 ± 0.0001	93.4 ± 2.8	0.0342 ± 0.0008	90.8 ± 0.4	0.0361 ± 0.0008
Coll–CTS 1 : 1	0.0055 ± 0.0001	88.7 ± 1.4	0.0487 ± 0.0007	90.9 ± 1.2	0.0603 ± 0.0009

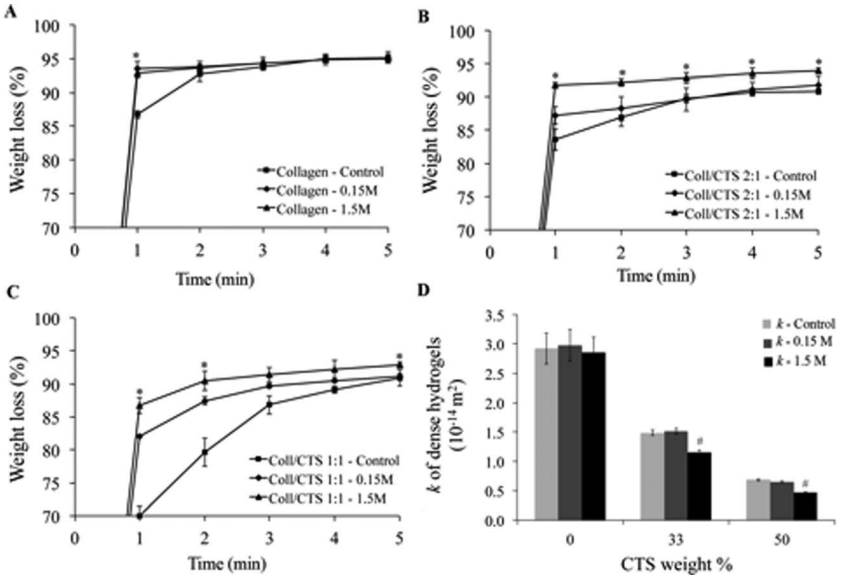

Fig. 5 Electrokinetic effect of CTS on the weight loss (%) and hydraulic permeability (k) properties of Coll (A), Coll–CTS 2 : 1 (B) and Coll–CTS 1 : 1 (C) hydrogels undergoing PC without pre-conditioning (control) and pre-conditioned in isotonic (0.15 M NaCl) and hypertonic (1.5 M NaCl) solutions. There was a decrease in weight loss after 5 min of PC with CTS content under both isotonic and hypertonic conditions ($p < 0.05$). There was no significant difference in Coll weight loss after 5 min PC in control, isotonic and hypertonic conditions. Coll–CTS 2 : 1 and Coll–CTS 1 : 1 hybrid gels demonstrated a significant increase in equilibrium weight loss with increasing NaCl concentration. (D) Charge screening by pre-equilibrating scaffolds in a high salt concentration solution resulted in no significant difference in Coll k values ($p > 0.05$) and up to 29% decrease in Coll–CTS dense hydrogels. There was no significant difference between control and isotonic conditions in all scaffolds formulations. * indicates a significant difference ($p < 0.05$) compared to previous time point. # indicates a significant difference ($p < 0.05$) compared to control. Data represented as mean ± SD, $n = 3$.

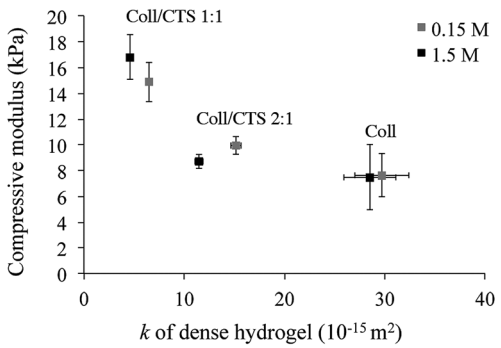

Fig. 6 Relationship between hydrogel compressive modulus and hydraulic permeability (k). Cylindrically shaped dense hydrogels were pre-equilibrated in an isotonic or hypertonic solution for 1 day prior compression testing. There was a significant increase in compressive modulus with CTS content under both conditions ($p < 0.05$). An increase in CTS content also resulted in a concomitant decrease in k. Data represented as mean ± SD, $n = 3$.

increase in ρ_{bead}, stabilizing at the equilibrium state. A gradient in bead density was observed from the bottom to the top of the scaffolds in accordance with a previous study using protein staining (Coomassie blue) to visualize collagen density during PC of highly hydrated Coll hydrogels.[25]

Increasing CTS content resulted in a greater difference in bead density between the top and bottom regions of hydrogels undergoing SC, suggesting that Coll gel structure is more uniform at equilibrium when compared to Coll–CTS hydrogels. Differences in bead density between the top and bottom regions of hybrid gels may be explained by an increase in the overall stiffness of the hydrogel[16,27] in the presence of CTS (as demonstrated by the 1.9-fold increase in the compressive modulus of Coll–CTS 1 : 1 compared to Coll alone), which influences the mechanism of densification during the gravity-driven consolidation process. In particular, at a microstructural level, CTS is thought to interlink with the collagen network (similar to native GAGs),[38] and increase the swelling pressure due to the repulsive forces between the fixed charged groups of the hydrogel, resulting in higher compressive modulus.[39,40] Since increasing the CTS content in Coll hydrogels results in greater stiffness, it was therefore hypothesized that ρ_{bead} throughout the hydrogel would decrease when undergoing SC. Indeed, the fold increase in density of Coll hydrogels decreased relative to CTS content. It is noteworthy that ρ_{bead} at equilibrium corresponded with the solid weight percent gravimetrically measured pre- and post-freeze drying. The correspondence between the beads and solid densities for each specimen validates the fluorescent bead imaging method as an effective and reliable indicator of solid density. Moreover, monitoring the position of fluorescent beads at different time points during the consolidation process provided an accurate measurement of bead position in space and time, offering an advantage over a previously published method based on collagen immunoreactivity which depends on homogeneous antibody binding and fluorescent intensity stability at greater depths in the scaffold.[23]

Under PC, and as early as 1 min, all formulations exhibited an increase in ρ_{bead} in the top and bottom regions. Following 1 min of compression, comparison of ρ_{bead} measured at the top 20 μm and bottom 80 μm of the scaffolds demonstrated no

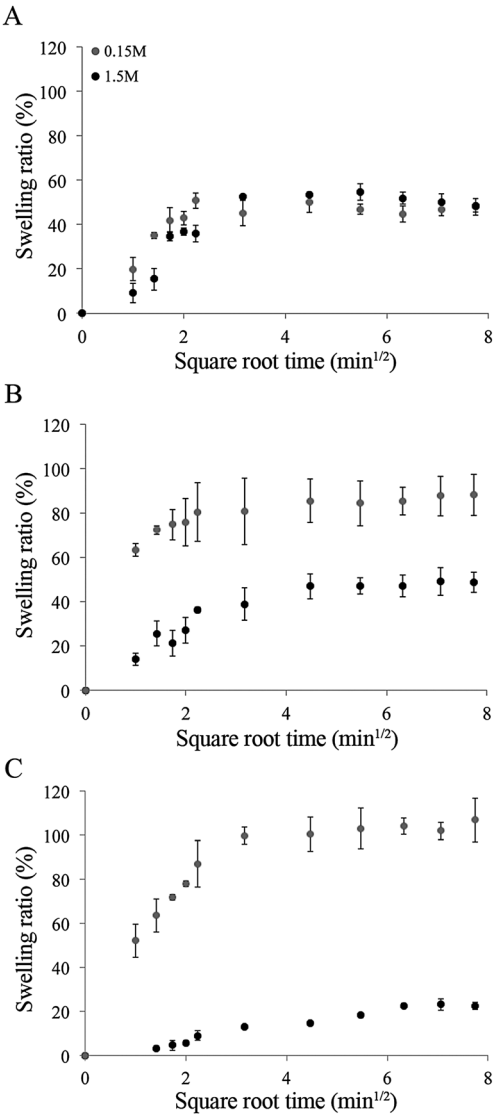

Fig. 7 Influence of CTS on hydrogel swelling in isotonic and hypertonic conditions. Swelling of dense Coll (A), Coll–CTS 2 : 1 (B) and Coll–CTS 1 : 1 (C) hydrogels were analyzed for up to 60 min. There was a decrease in swelling ratio with increasing CTS content under hypertonic conditions. Data represented as mean ± SD, $n = 4$.

significant difference ($p > 0.05$). Analogous to SC, the final density within the bottom 80 μm of all scaffolds corresponded with both the densities of SC gels at equilibrium and with the solid weight percent of PC gels obtained by the freeze-drying method. However, the final density at the bottom 20 μm of the PC Coll gels was 49% higher compared to the top and bottom 80 μm. This phenomenon can be attributed to the application of an external stress resulting in the accumulation of collagen fibrils at the gels FEB due to higher fluid flow (10-fold increase in weight loss rate under PC, compared to SC) and the unstable physical structure of the hydrogel.[24] In contrast, there was no significant difference between the three analyzed regions in Coll–CTS hydrogels at the equilibrium state, therefore suggesting a uniformly distributed solid density throughout the scaffolds thickness, compared to the gravity-driven process. Since positively charged CTS contains several hydrophilic groups, such as hydroxyl, amino and carboxyl groups, it promotes water entrapment within the hydrogel, therefore reducing the fluid flow,[41] and consequently the solid density throughout the scaffold thickness, as demonstrated by the reduction in the rate and final weight loss of Coll–CTS 1 : 1 gels compared to Coll–CTS 2 : 1 and Coll alone.

The Happel model is a generalized microstructurally based model for the calculation of k, a property that can be correlated with the inflow of nutrients and oxygen as well as the outflow of metabolic waste and biodegradation by-products within a hydrogel.[42] The Happel model describes the flow resistance as a summation of the resistance of cylindrical rods parallel and perpendicular to the flow,[5] and has been particularly useful in tissues such as articular cartilage[32,33] and fibrillar materials such as collagen, where collagen is modelled as a long cylindrical fibre.[26] Since this model assumes a constant rod cross-sectional area along the direction of the flow, and GAG chains are the most critical determinant of the permeability in native cartilage (based on previous measurements), the Happel model has been used to calculate cartilage permeability by modelling GAG chains as rods of a constant radius "a" and assuming that the contribution of collagen to flow resistance is negligible.[10,26,32,43] Since the microstructural properties are considered as one of the major signaling sources regulating cell growth and differentiation, further studies of hydrogel k properties are critical.[44] In analogy to cartilage, in this study, CTS – a polysaccharide of structural similarity to GAGs found in native ECM – was also modelled as a rod-like structure of a hydrodynamic radius of 39 nm,[31] which in combination with experimentally measured solid volume fraction values, allowed the calculation of Coll–CTS permeability. The analysis revealed decreasing k values in hydrogels with higher CTS content both in highly hydrated and dense forms, analogous to proteoglycans in articular cartilage.[45] A plausible explanation may be that an increase in fixed charge density, which originates from the protonated amino groups found in the polysaccharide structure, lowers the content of water that is free and therefore k.[46]

In connective tissues, collagen itself is essentially neutral at physiological pH (isoelectric point at pH 7.5), whereas GAG chains possesses one to two fixed negative charges per disaccharide unit, generating the bulk flow through the interstitium to induce streaming potentials.[45,47] In the present study, the electrostatic contribution of CTS to Coll hydrogels was investigated through structural, mechanical and swelling characterizations under isotonic and hypertonic conditions.[48] Elimination of the screening charges with high concentrations of salts (hypertonic) resulted in no significant effect on Coll hydrogel k ($p > 0.05$). This is in contrast to dense Coll–CTS gels, which presented up to 29% reduction in k. This suggests that the electrokinetic effect does not account for the majority of the Coll–CTS k and that the determinant factor is the tortuosity flow-path induced by the interlinked CTS within the collagen network. The k values obtained in this study for dense Coll hydrogels corresponded to those previously published for Coll gel scaffolds (1×10^{-15}–10^{-16} m^2)[49] and 3 orders of magnitude higher compared to human articular cartilage

($\sim$0.1–2 $\times$ 10^{-18} m^2).[50] In addition, with decreasing k, there was a concomitant increase in the compressive modulus of the scaffolds with CTS under both isotonic and hypertonic conditions, which can be explained by CTS fixed charge increasing the osmotic pressure and resistance to compressive forces.[51]

Under isotonic conditions, increasing amounts of CTS resulted in higher swelling ratios. This increment was attributed to the increased number of protonated groups, which augment the repulsive forces between the fixed charged constituents of the hydrogel, resulting in greater osmotic pressure and promotion of water intake.[39,40] Increasing the concentration of salt resulted in a decrease in swelling ratio of Coll–CTS hydrogels, while the Coll gels remained unchanged. A likely mechanism for Coll–CTS swelling reduction is the salt's ability to increase the degree of screening of fixed charge, leading to a reduction in electrostatic repulsion and of the osmotic pressure, therefore, restricting the capacity for hydrogels to swell.[39]

The ability of CTS to control and tune the permeability, mechanical and swelling properties of a biomimetic scaffold such as dense Coll hydrogels, may be utilized for various applications, including drug delivery and TE. For example, charged hydrogels have been shown to be effective drug carriers, which are able to release entrapped pharmaceutical drugs in response to a swelling trigger.[52] In addition, the positively charged molecules may facilitate cell differentiation by electrostatically binding cell membrane and negatively charged GAGs.[53,54] In fact, it has been observed that increasing CTS content within dense Coll gels has a stimulatory effect towards the chondrocytic lineage, revealing that CTS plays an important role in stimulating ECM production.[27] Moreover, this *in vitro* model may also be used as a simple tool to measure the interaction of connective tissue GAGs with collagen, as well as with cell surfaces through a receptor-like mechanism.[45]

5. Conclusion

In this study, the effect of CTS on the microstructural evolution involved in SC and PC of highly hydrated Coll–CTS hydrogels was investigated by monitoring the spatiotemporal distribution of fluorescent beads by CLSM. Measured final bead density and solid weight percent values corresponded closely, thus validating this fluorescent-based imaging method. CTS fixed charge effect on dense Coll–CTS hydrogels was analyzed through structural (*i.e.* hydraulic permeability), mechanical and swelling characterizations under isotonic and hypertonic conditions. The results indicated the ability of a charged GAG-analog to control the physicochemical properties of Coll hydrogels, offering the potential for tailoring scaffolds for TE and other biomedical applications.

Acknowledgements

This work was supported by funds from Canadian Natural Sciences and Engineering Research Council, the Canadian Foundation for Innovation, and the McGill University Faculty of Engineering Gerald Hatch Faculty Fellowship (in support of SNN). Florencia Chicatun is also partly supported by McGill Engineering Doctoral Awards, Vadasz and Hatch fellowships and a Bourses Fondation Pierre Arbour scholarship.

References

1 L. G. Griffith and G. Naughton, *Science*, 2002, **295**, 1009–1014.
2 L. G. Griffith and M. A. Swartz, *Nat. Rev. Mol. Cell Biol.*, 2006, **7**, 211–224.
3 P. Fratzl, *Collagen: structure and mechanics*, Springer Science + Bussiness Media, LLC, New York, 2008.
4 D. G. Wallace and J. Rosenblatt, *Adv. Drug Delivery Rev.*, 2003, **55**, 1631–1649.
5 M. A. Swartz and M. E. Fleury, *Annu. Rev. Biomed. Eng.*, 2007, **9**, 229–256.
6 J. A. Burdick and R. L. Mauck, *Biomaterials for tissue engineering applications: a review of the past and future trends*, Springer-Verlag, Germany, 2011.
7 M. S. Laasanen, J. Toyras, R. K. Korhonen, J. Rieppo, S. Saarakkala, M. T. Nieminen, J. Hirvonen and J. S. Jurvelin, *Biorheology*, 2003, **40**, 133–140.
8 G. E. Kempson, H. Muir, S. A. V. Swanson and M. A. R. Freeman, *Biochim. Biophys. Acta*, 1970, **215**, 70–77.
9 W. Y. Gu and H. Yao, *Ann. Biomed. Eng.*, 2003, **31**, 1162–1170.
10 J. R. Levick, *Q. J. Exp. Physiol. Cogn. Med. Sci.*, 1987, **72**, 409–438.
11 A. R. Costa-Pinto, R. L. Reis and N. M. Neves, *Tissue Eng., Part B*, 2011, **17**, 331–347.
12 J. K. F. Suh and H. W. T. Matthew, *Biomaterials*, 2000, **21**, 2589–2598.
13 A. Lahiji, A. Sohrabi, D. S. Hungerford and C. G. Frondoza, *J. Biomed. Mater. Res.*, 2000, **51**, 586–595.
14 M. Navarro, A. Michiardi, O. Castano and J. A. Planell, *J. R. Soc., Interface*, 2008, **5**, 1137–1158.
15 S. Bhat, A. Tripathi and A. Kumar, *J. R. Soc., Interface*, 2011, **8**, 540–554.
16 F. Chicatun, C. E. Pedraza, C. E. Ghezzi, B. Marelli, M. T. Kaartinen, M. D. McKee and S. N. Nazhat, *Biomacromolecules*, 2011, **12**, 2946–2956.
17 L. M. Wang and J. P. Stegemann, *Biomaterials*, 2010, **31**, 3976–3985.
18 W. Tan, R. Krishnaraj and T. A. Desai, *Tissue Eng.*, 2001, **7**, 203–210.
19 B. Sun, W. Ma, F. Su, Y. Wang, J. Liu, D. Wang and H. Liu, *J. Mater. Sci.: Mater. Med.*, 2011, **22**, 2111–2118.
20 K. D. Song, M. Qiao, T. Q. Liu, B. Jiang, H. M. Macedo, X. H. Ma and Z. F. Cui, *J. Mater. Sci.: Mater. Med.*, 2010, **21**, 2835–2842.
21 R. A. Brown, M. Wiseman, C. B. Chuo, U. Cheema and S. N. Nazhat, *Adv. Funct. Mater.*, 2005, **15**, 1762–1770.
22 E. A. Abou Neel, U. Cheema, J. C. Knowles, R. A. Brown and S. N. Nazhat, *Soft Matter*, 2006, **2**, 986–992.
23 V. Serpooshan, T. M. Quinn, N. Muja and S. N. Nazhat, *Soft Matter*, 2011, **7**, 2918–2926.
24 V. Serpooshan, T. M. Quinn, N. Muja and S. N. Nazhat, *Acta Biomater.*, 2013, **9**, 4673–4680.

25 E. Hadjipanayi, M. Ananta, M. Binkowski, I. Streeter, Z. Lu, Z. F. Cui, R. A. Brown and V. Mudera, *J. Tissue Eng. Regener. Med.*, 2011, **5**, 505–519.
26 J. Happel, *AIChE J.*, 1959, **5**, 174–177.
27 F. Chicatun, C. E. Pedraza, N. Muja, C. E. Ghezzi, M. D. McKee and S. N. Nazhat, *Tissue Eng., Part A*, 2013, DOI: 10.1089/ten.tea.2013.0114.
28 V. Serpooshan, M. Julien, O. Nguyen, H. F. Wang, A. L. Li, N. Muja, J. E. Henderson and S. N. Nazhat, *Acta Biomater.*, 2010, **6**, 3978–3987.
29 G. Fels, *J. Appl. Polym. Sci.*, 1964, **8**, 1863.
30 Y. I. Cho, H. K. No and S. P. Meyers, *J. Agric. Food Chem.*, 1998, **46**, 3839–3843.
31 O. Mertins and R. Dimova, *Langmuir*, 2011, **27**, 5506–5515.
32 A. Maroudas, *Ann. Rheum. Dis.*, 1975, **34**, 77–81.
33 A. J. Grodzinsky, *Crit. Rev. Biomed. Eng.*, 1983, **9**, 133–199.
34 H. C. Chin, G. Khayat and T. M. Quinn, *J. Biomech.*, 2011, **44**, 198–201.
35 B. Marelli, C. E. Ghezzi, J. E. Barralet, A. R. Boccaccini and S. N. Nazhat, *Biomacromolecules*, 2010, **11**, 1470–1479.
36 H. Park, X. Guo, J. S. Temenoff, Y. Tabata, A. I. Caplan, F. K. Kasper and A. G. Mikos, *Biomacromolecules*, 2009, **10**, 541–546.
37 K. Kawasaki, A. V. Buchanan and K. M. Weiss, *Annu. Rev. Genet.*, 2009, **43**, 119–142.
38 A. Maroudas, *Nature*, 1976, **260**, 808–809.
39 S. R. Eisenberg and A. J. Grodzinsky, *J. Orthop. Res.*, 1985, **3**, 148–159.
40 V. C. Mow, A. Ratcliffe and A. R. Poole, *Biomaterials*, 1992, **13**, 67–97.
41 C. R. Correia, L. S. Moreira-Teixeira, L. Moroni, R. L. Reis, C. A. van Blitterswijk, M. Karperien and J. F. Mano, *Tissue Eng., Part C*, 2011, **17**, 717–730.
42 C. M. Agrawal and R. B. Ray, *J. Biomed. Mater. Res.*, 2001, **55**, 141–150.
43 T. M. Quinn, P. Dierickx and A. J. Grodzinsky, *J. Biomech.*, 2001, **34**, 1483–1490.
44 S. C. Owen and M. S. Shoichet, *J. Biomed. Mater. Res., Part A*, 2010, **94**, 1321–1331.
45 W. D. Comper and T. C. Laurent, *Physiol. Rev.*, 1978, **58**, 255–315.
46 A. Maroudas, *Biophys. J.*, 1968, **8**, 575–595.
47 W. M. Lai, V. C. Mow, D. D. Sun and G. A. Ateshian, *J. Biomech. Eng.*, 2000, **122**, 336–346.
48 C. Canal Guterl, C. T. Hung and G. A. Ateshian, *J. Biomech.*, 2010, **43**, 1343–1350.
49 S. Ramanujan, A. Pluen, T. D. McKee, E. B. Brown, Y. Boucher and R. K. Jain, *Biophys. J.*, 2002, **83**, 1650–1660.
50 F. J. O'Brien, B. A. Harley, M. A. Waller, I. V. Yannas, L. J. Gibson and P. J. Prendergast, *Technol. Health Care*, 2007, **15**, 3–17.
51 R. K. Korhonen, P. Julkunen, W. Wilson and W. Herzog, *J. Biomech. Eng.*, 2008, **130**, 021003.
52 J. Ostroha, M. Pong, A. Lowman and N. Dan, *Biomaterials*, 2004, **25**, 4345–4353.
53 M. Dadsetan, M. Pumberger, M. E. Casper, K. Shogren, M. Giuliani, T. Ruesink, T. E. Hefferan, B. L. Currier and M. J. Yaszemski, *Acta Biomater.*, 2011, **7**, 2080–2090.
54 S. J. Bryant, J. A. Arthur and K. S. Anseth, *Acta Biomater.*, 2005, **1**, 243–252.